30p

code-1

NASA TN D-1800

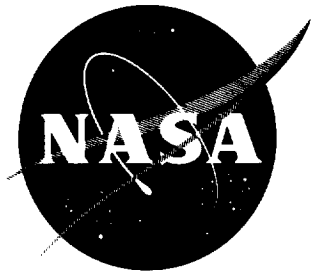

TECHNICAL NOTE

D-1800

AERODYNAMIC INTERACTION EFFECTS AHEAD OF RECTANGULAR SONIC JETS EXHAUSTING PERPENDICULARLY FROM A FLAT PLATE INTO A MACH NUMBER 6 FREE STREAM

By David J. Romeo

Langley Research Center
Langley Station, Hampton, Va.

NATIONAL AERONAUTICS AND SPACE ADMINISTRATION
WASHINGTON May 1963

Code-1

NATIONAL AERONAUTICS AND SPACE ADMINISTRATION

TECHNICAL NOTE D-1800

AERODYNAMIC INTERACTION EFFECTS AHEAD OF RECTANGULAR SONIC JETS EXHAUSTING PERPENDICULARLY FROM A FLAT PLATE INTO A MACH NUMBER 6 FREE STREAM

By David J. Romeo

SUMMARY

The aerodynamic interaction effects ahead of a three-dimensional rectangular jet exhausting perpendicularly from a flat plate have been investigated at a free-stream Mach number of 6. The test was made at an angle of attack of 0°, at a Reynolds number per foot of approximately 6.5×10^6, and with a turbulent boundary layer on the plate. The ratio of jet total pressure to free-stream static pressure was varied from approximately 20 to 440, the jet slot width varied from 0.001 to 0.100 inch, and the jet slot span varied from 0.20 to 2.00 inches. The interaction pressure distribution ahead of the slot center line was similar to and quantitatively approached the results of a two-dimensional jet slot as the slot width, slot span, and jet pressure ratio were increased. The ratio of aerodynamic normal force to reaction normal force decreased slightly with increasing jet pressure ratio for the largest jet slot widths, but this trend was reversed as the jet slot width was decreased (i.e., for the smaller slot widths, the ratio increased with increasing jet pressure ratio). In general, the largest values of the ratio of aerodynamic normal force to reaction normal force were found for the smallest jet slot widths and largest jet pressure ratios. The aerodynamic normal-force coefficient was comparable to two-dimensional results when the aspect ratio of the jet was kept above a value dictated by the slot width. This value of the ratio of slot span to slot width increased rapidly as slot width decreased.

INTRODUCTION

Aerodynamic interaction effects associated with a jet exhausting perpendicularly from a flat plate have already been investigated at a Mach number of 6 for the case of two-dimensional spanwise slots. (See ref. 1.) At lower Mach numbers, this effect has also been explored to some degree for both two- and three-dimensional models. (See refs. 2 to 8.) Reference 3, for example, has shown that significant aerodynamic normal forces could be obtained in some cases for a three-dimensional jet exhausting perpendicularly from the rear of a cylindrical body. In addition, tests of reference 1 indicated that it was possible to obtain high values of the ratio of aerodynamic normal force to jet reaction normal force for cases of relatively small jet slot widths and large jet pressure ratios.

In view of the encouraging results of reference 1, it was decided to extend this investigation to a series of three-dimensional rectangular jets exhausting perpendicularly from a wide flat plate. More specifically, the present paper provides information for the prediction of the amount of aerodynamic normal force that may be obtained ahead of a rectangular sonic jet, over a wide range of jet slot widths and jet slot spans for the boundary-layer conditions of these tests. The tests were conducted at a free-stream Mach number of 6 for a wide range of jet total pressures. The entire investigation was conducted for conditions of a turbulent boundary layer ahead of the jet and with the plate alined with free-stream flow.

SYMBOLS

$C_{N,A}$ integrated normal-force coefficient on plate due to aerodynamic interaction of jet, $\int l_y \int l_x \frac{p - p_\infty}{qS} dx\, dy$

$C_{N,R}$ calculated normal-force coefficient due to reaction of jet alone, $\left[\frac{(\gamma M_j^2 + 1)p_j - p_\infty}{qS}\right] sd$

$\Delta C_{N,A}$ amount of normal-force coefficient outboard of slot span

d slot width, in.

l_x axial length of separated region, in.

l_y spanwise length of separated region, in.

M Mach number

N_R calculated reaction normal force, $C_{N,R}qS$

p pressure, lb/sq in. abs

q dynamic pressure, lb/sq in. abs

S reference area, slot span times distance from plate leading edge to jet slot, sq in.

s slot span, in.

x lengthwise distance measured from foremost orifice, positive rearward, in. (see fig. 1)

y spanwise distance measured from foremost orifice, in. (see fig. 1)

γ ratio of specific heats

Subscripts:

j jet-exit conditions

max maximum

t,j jet stagnation conditions

2-D two-dimensional

∞ free-stream test-section conditions

APPARATUS

Wind Tunnel

This program was carried out in the Langley 20-inch Mach 6 tunnel. The tunnel is a blowdown-to-atmosphere type and was operated at a stagnation pressure of approximately 340 lb/sq in. abs at a stagnation temperature of 400° F. The corresponding Reynolds number per foot was 6.5×10^6. A more complete description of the tunnel is presented in reference 9.

Models and Supports

The basic model used in this program consisted of a flat plate 10 inches wide with a 10° leading-edge wedge that tapered to a maximum radius of 0.001 inch at the leading edge. The length of the model from the leading edge to the front of the jet slot was 14 inches.

Sixty-one 0.060-inch-inside-diameter pressure orifices were installed on the plate and positioned as shown in figure 1. Figure 1 also shows the general dimensions of the plate and the four inserts that were used to obtain the different slot spans. Steel shims were used to vary the slot widths for the different inserts. The inserts were held by means of capscrews at the side, rear, and through the bottom of the plate. Compressed air was supplied to the model by means of a 1-inch-diameter tube entering through the bottom of the tunnel and into a chamber between the insert and plate. The chamber total pressure was controlled by means of a $1\frac{1}{2}$-inch globe valve and a 1-inch needle valve placed in parallel in the air line. The whole model was rigidly supported by three struts mounted on the tunnel floor. Figure 2 is a photograph of the model mounted in the tunnel. Shown in the figure are the struts and the sheet-metal shroud that was placed on the underside of the model for streamlining purposes. Also shown is a roughness strip that was used for tripping the flow (insuring transition). The strip was

about 3/4 inch wide, had a maximum height of approximately 0.05 inch, and spanned the plate $1\frac{1}{4}$ inches from the leading edge.

TEST METHODS AND TECHNIQUES

The 61 static-pressure leads were attached to six pressure switching devices which fed the pressures in sequence to electrical pressure transducers. The transducer outputs were recorded on magnetic tape by means of a commercial digital readout system.

Each orifice was connected to both a 0-1 and a 0-5 lb/sq in. abs pressure transducer in order to obtain necessary range and maximum accuracy. The accuracy of the transducers was 1 percent of full-scale reading. The most extreme spanwise orifice locations were monitored during the running of the tests to be certain that the interaction effects were contained within the width of the plate. The jet chamber total pressure was measured on a 0-100 lb/sq in. gage transducer, and was also recorded on the magnetic tape. The static pressures were recorded for each incremental change in jet total pressure for each run.

From a previous program (ref. 1), it was known that with roughness on the plate the boundary layer that existed in the plane of the jet without jet flow was fully turbulent. The boundary-layer displacement thickness at this point was approximately 0.14 inch.

Two methods for obtaining the integrated normal-force coefficients were used. The first method consisted of assigning an incremental area to each orifice, multiplying the area by the pressure difference between the reading and the tare value, and summing the incremental forces. This method was rapid since it could be performed entirely by machine computation. The second method consisted of mechanically integrating curves of plotted pressure distribution in both the axial and spanwise directions. This method was more tedious than the first and was used primarily as a check for the larger values of normal-force coefficient, where it was found that the two methods were in close agreement. The results of the second method, however, were used exclusively for some of the very small values of $C_{N,A}$ where it was believed that the first method became inadequate. Values of $C_{N,A}$ obtained by both methods are shown on the data plots.

RESULTS AND DISCUSSION

Surface Pressure Distribution

The issuance of a secondary jet into a supersonic stream always causes a disruption of the main stream flow at the jet. Since the jet flow usually causes the boundary layer on the surface from which the jet is exhausting to separate, the influence often is also felt some distance upstream. Typical results of this aerodynamic interaction in terms of surface pressure distribution ahead of the jet are presented in figures 3 to 6. (See fig. 12 for a sketch of the pressure

distribution.) Figures 3 and 4 show typical center-line distributions and figures 5 and 6 illustrate the effect of the three-dimensionality of the rectangular jet slots. It should be kept in mind that the results shown apply only to the surface that is ahead or upstream of the jet.

Figure 3 shows the effect of increasing the jet pressure ratio on the center-line pressure distribution for a typical slot span and slot width. It can be seen that although the disturbance distance increases as the jet pressure ratio is increased, the initial pressure rise remains similar in basic pattern or shape. Also of interest is the fact that the first peak pressure increases very little as the jet pressure ratio is increased. The results here are similar to those observed in reference 1 for a two-dimensional jet slot. Figure 4 shows the effect of increasing the jet slot width d on the center-line pressure distribution for a constant value of jet pressure ratio and slot span. The first peak pressure increases slightly as the slot width is increased.

An example of the spanwise decay in the separated region ahead of the jet as the distance from the jet center line is increased is shown in figure 5. For this case, the edge of the jet slot is at $y = 1.0$ inch and it can be seen that the pressure distribution profile retains its shape out to this distance. Farther outboard, the first peak pressure drops off rapidly and the contour loses its characteristic appearance. Also shown is the fact that the axial position of the first peak moves rearward as the position of the contour is examined farther out from the center line (i.e., as y increases).

The effect of slot span s on the extent of separation at the jet center line for a constant jet pressure ratio and slot width is illustrated in figure 6. Included in this figure for comparison are the surface pressure distributions for a two-dimensional jet slot (ref. 1) and a forward-facing step (ref. 9), both of which are for the same test conditions of this program. Increasing the slot span increases the separated region and also slightly increases the first peak pressure, and both of these values appear to be approaching the two-dimensional jet-slot values as the span is increased. It was found in reference 1 that the jet pressure ratio and jet slot width had only a small effect on the first peak pressure and that the value of the first peak pressure was approximately equal to the value ahead of the forward-facing step. (Ref. 9 has shown that where a step height is larger than the boundary-layer thickness in turbulent flow, the first peak pressure does not change significantly with step height.) The trends illustrated in the present investigation are then comparable to the two-dimensional results.

Aerodynamic and Reaction Normal-Force Coefficients

Figures 7 and 8 show the effect of jet pressure ratio on the aerodynamic normal-force coefficient $C_{N,A}$ and on the ratio of aerodynamic normal-force coefficient to reaction normal-force coefficient $C_{N,A}/C_{N,R}$ for the range of slot widths and slot spans of this investigation. The aerodynamic normal-force coefficients $C_{N,A}$ were calculated by the methods described in the section entitled "Test Methods and Techniques." The jet-reaction normal-force coefficients

$C_{N,R}$ were calculated by the theoretical formula given in the symbol list, where the jet Mach number at the exit was assumed to be sonic and the exit area was determined without correction for jet boundary layer. As mentioned in the previous section, when considering the data it is important to remember that the aerodynamic interaction was calculated for forces upstream of the jet and the results must not be confused with a case in which the forces downstream of the jet are also considered in the net interaction. This precautionary statement is necessitated by the large difference in the results that could be obtained if both upstream and downstream forces were considered. (See, for example, refs. 2 and 3.) Thus, for use as a control device, the jet is assumed to be located at the trailing edge of a planar wing.

Figure 7 shows that the increase of $C_{N,A}$ with $p_{t,j}/p_\infty$ is nearly linear over the test range for any one slot width and slot span. Comparing the effect of slot width d for a given span s, however, shows that a reduction in slot width at a given pressure ratio, in general, does not give a proportional reduction in $C_{N,A}$; that is, the smaller slot widths are more productive in proportion to their size than the larger widths. Decreasing the slot width d from 0.100 inch to 0.050 inch (for example, see fig. 7(b)) reduces the value of $C_{N,A}$ by less than 50 percent, and, in general, as d is decreased even further, the relative reduction in $C_{N,A}$ becomes proportionately less.

The relative gain (normal force per unit slot width) in $C_{N,A}$ as d decreases is perhaps more clearly evident in figure 8, which shows $C_{N,A}/C_{N,R}$ plotted against $p_{t,j}/p_\infty$. In this figure, it is seen that the largest ratios of $C_{N,A}/C_{N,R}$ generally occur for the smallest slot widths and at the largest jet pressure ratios. These trends have already been noted for the two-dimensional case in reference 1, and the present data verify the two-dimensional results and extend them to the three-dimensional cases of rectangular slots. Another item of considerable interest is the way in which $C_{N,A}/C_{N,R}$ varies with jet pressure ratio. In some of the other investigations of jet aerodynamic interaction (for example, ref. 3), it was felt that an increase in jet pressure ratio $p_{t,j}/p_\infty$ would result in a decrease in $C_{N,A}/C_{N,R}$. An inspection of figure 8(b), for example, shows that at the largest slot width of the test, the value of $C_{N,A}/C_{N,R}$ does decrease slightly with increasing $p_{t,j}/p_\infty$; however, as the slot width is decreased, the variation of $C_{N,A}/C_{N,R}$ with $p_{t,j}/p_\infty$ changes in trend. At the smallest values of slot width, $C_{N,A}/C_{N,R}$ increases rapidly with increase in $p_{t,j}/p_\infty$. Evidently then, the slot width d, or perhaps more properly the ratio of slot width to boundary-layer displacement thickness or some other characteristic dimension of the boundary layer, must be considered when attempting to predict this trend.

Figure 8 showed that a decrease in jet slot width d generally produced an increase in $C_{N,A}/C_{N,R}$; but it gave no indication as to how the gross values of normal force varied, since for a constant span, a decrease in slot width would necessarily cause a decrease in reaction normal-force coefficient $C_{N,R}$. Figure 9

shows the normal-force-coefficient ratio as a function of pure reaction normal force N_R for a typical jet pressure ratio and for the range of test slot widths. This type of plot would be useful if the exit geometry of a reaction jet that would give maximum total normal force was being sought and the maximum available reaction force was already known. This example shows that for the slots used in this investigation at a given value of N_R, the smallest slot widths are the most effective. Since for a constant pressure ratio the mass flow is also directly proportional to the slot width, constant values of N_R can also be thought of as constant values of jet mass flow and the figure may be interpreted with this in mind.

A similarity in the trends of the results of this investigation with the two-dimensional tests has been established but there remains the question of how well the aerodynamic interactions for the three-dimensional jet slots compare quantitatively with the two-dimensional results of reference 1. Figure 10 is a cross plot that shows the effect of slot span s on normal-force coefficient $C_{N,A}$ for the range of jet slot widths and for a representative jet pressure ratio. This figure shows that at the smaller values of slot width the maximum values of $C_{N,A}$ occurred for $s = 1.00$ inch. Included in the figure are the two-dimensional results of reference 1. It can be seen that $C_{N,A}$ is approximately equal to the two-dimensional value for the larger slot spans but, as the slot span decreases, at some particular value of s depending on slot width, the value of $C_{N,A}$ begins to fall off very rapidly. Therefore it can be concluded that the three-dimensional slot yields values of $C_{N,A}$ comparable to the two-dimensional case for some particular value of slot span s, or larger.

For the purpose of comparing what values of span s or aspect ratio s/d are needed for near two-dimensional results, it was arbitrarily decided to look at values of $C_{N,A}$ which were 75 percent of the two-dimensional results. For the representative pressure ratio of figure 10 and for four other values not shown, values of s at which $C_{N,A}$ is 75 percent of $C_{N,A}$ for a two-dimensional slot were found for each slot width. These data are presented in figure 11 in terms of aspect ratio s/d plotted against slot width d. The figure shows that the values of s/d obtained are a strong function of jet slot width d but change little with jet pressure ratio $p_{t,j}/p_\infty$. Therefore, a single curve was faired through the data points for the values of jet pressure ratio presented. The curve illustrates that for any value of slot width d, it is possible to obtain an aspect ratio s/d which will give values of $C_{N,A}$ that are 75 percent or more of the two-dimensional values by choosing a value on or above the curve. The curve also shows that this value of s/d increases very rapidly as d decreases.

A possible explanation of why the value of s/d for 75 percent or more of $(C_{N,A})_{2\text{-}D}$ is such a strong function of slot width d is now given with the use of figures 12 and 13.

Figure 12 is a sketch given for the purpose of illustrating the affected surface areas for the two- and three-dimensional interaction cases. The shaded areas define the regions used to determine $C_{N,A}$ and $\Delta C_{N,A}$. The entire shaded region

is used to determine $C_{N,A}$ and the doubled shaded region outboard of the jet slots is used to determine $\Delta C_{N,A}$. It can be seen from the sketch and also from figure 6 that the three-dimensional interaction region is smaller than the two-dimensional region directly in front of the jet slot, but that the three-dimensional interaction force will gain some effect $\left(\Delta C_{N,A}\right)$ on both sides of the jet slot and this gain will provide an appreciable fraction of the total force. In the sketch showing the three-dimensional interaction, the areas marked "loss" and "gain" refer to the difference between the affected areas for the two- and three-dimensional jet slots. As any slot span becomes more three-dimensional (i.e., as s/d decreases), both the gain outboard and loss in front in the affected area should increase, but not necessarily at the same rate. Conceivably then, there could be a value of s/d for $\left(C_{N,A}\right)_{max}$ for any given slot width that would be even greater than the two-dimensional value, and this value may be the one corresponding to the slot span that gives the largest values of $C_{N,A}$ ($s = 1.00$ inch for values of $d < 0.010$ inch in these tests). Figure 10 indicates that maximum values of $C_{N,A}$ exist for given slot widths; however, these values are, in general, approximately equal to the two-dimensional values so that this result does not appear to be of serious significance at the present time.

The value of $\Delta C_{N,A}/C_{N,A}$ for a typical jet pressure ratio is shown in figure 13. For a given slot width, $\Delta C_{N,A}/C_{N,A}$ decreases as the aspect ratio s/d increases, as would be expected. More important, however, this figure shows that equivalent interaction patterns $\left(\text{i.e., } \Delta C_{N,A}/C_{N,A} = \text{Constant}\right)$ occur at different values of s/d for different values of slot width d. In other words, for a constant line or value of $\Delta C_{N,A}/C_{N,A}$, the value of s/d increases as d decreases. This observation could perhaps be the reason for the increase, as d decreases, in s/d for the 75 percent of $C_{N,A}$ two-dimensional line shown in figure 11.

In the previous discussion, it has been assumed that sufficient outboard surface exists to realize the total interaction effect $\left(C_{N,A}\right)$. Figure 14 shows the minimum surface span that would be required in order to obtain the total interaction force. As expected, the ratio of minimum required span to actual jet slot span $\left(l_y/s\right)$ decreases as s/d increases. This result tends to verify the trends deduced from figures 12 and 13.

CONCLUSIONS

The aerodynamic interaction ahead of a three-dimensional rectangular jet exhausting perpendicularly from a flat plate into a Mach number 6 free stream has been investigated. It has been concluded for the conditions of the tests that:

1. The three-dimensional interaction pressure rise ahead of the slot center line was similar to the pressure rise seen in two-dimensional jet investigations. The first peak pressure increased slightly with increasing jet slot width, jet slot span, and jet pressure ratio and approached the values found for a

two-dimensional jet (NASA TN D-743) and a two-dimensional forward-facing step (NASA TN D-618).

2. The ratio of aerodynamic normal force to pure reaction normal force decreased slightly with increasing jet pressure ratio for the largest jet slot widths, but this trend was reversed as the jet slot width was decreased (i.e., for the smaller slot widths, the ratio increased rapidly with increasing jet pressure ratio). In general, the largest values of the ratio of aerodynamic normal force to reaction normal force were found for the smallest jet slot widths and largest jet pressure ratios.

3. The aerodynamic normal-force coefficient was approximately equal to values for a two-dimensional jet slot when the aspect ratio was kept above a value dictated by the slot width. This value of the ratio of slot span to slot width increased rapidly as slot width decreased.

Langley Research Center,
National Aeronautics and Space Administration,
Langley Station, Hampton, Va., March 12, 1963.

REFERENCES

1. Romeo, David J., and Sterrett, James R.: Aerodynamic Interaction Effects Ahead of a Sonic Jet Exhausting Perpendicularly From a Flat Plate Into a Mach Number 6 Free Stream. NASA TN D-743, 1961.

2. Morkovin, M. V., Pierce, C. A., Jr., and Craven, C. E.: Interaction of a Side Jet With a Supersonic Main Stream. Bull. No. 35, Eng. Res. Inst., Univ. of Michigan, Sept. 1952.

3. Vinson, P. W., Amick, J. L., and Liepman, H. P.: Interaction Effects Produced by Jet Exhausting Laterally Near Base of Ogive-Cylinder Model in Supersonic Main Stream. NASA MEMO 12-5-58W, 1959.

4. Lowry, John G.: Recent Control Studies. NACA RM L55L22a, 1956.

5. Lord, Douglas R.: Aerodynamic Characteristics of Several Jet-Spoiler Controls on a 45° Sweptback Wing at Mach Numbers of 1.61 and 2.01. NACA RM L58D18, 1958.

6. Ferrari, Carlo: Interference Between a Jet Issuing Laterally From a Body and the Enveloping Supersonic Stream. Bumblebee Rep. No. 286 (Contract NOrd 7386), Appl. Phys. Lab., Johns Hopkins Univ., Apr. 1959.

7. Janos, Joseph J.: Loads Induced on a Flat-Plate Wing by an Air Jet Exhausting Perpendicularly Through the Wing and Normal to a Free-Stream Flow of Mach Number 2.0. NASA TN D-649, 1961.

8. Cubbison, Robert W., Anderson, Bernhard H., and Ward, James J.: Surface Pressure Distributions With a Sonic Jet Normal to Adjacent Flat Surfaces at Mach 2.92 to 6.4. NASA TN D-580, 1961.

9. Sterrett, James R., and Emery, James C.: Extension of Boundary-Layer-Separation Criteria to a Mach Number of 6.5 by Utilizing Flat Plates With Forward-Facing Steps. NASA TN D-618, 1960.

ORIFICE	x	y	ORIFICE	x	y
1	4.50	0.00	32	5.65	1.10
2	4.25	0.00	33	5.15	1.10
3	4.00	0.00	34	4.90	1.10
4	3.75	0.00	35	4.65	1.10
5	3.50	0.00	36	4.50	1.10
6	3.00	0.00	37	4.15	1.10
7	2.50	0.00	38	3.65	1.10
8	2.00	0.00	39	4.65	1.30
9	1.50	0.00	40	4.50	1.30
10	1.00	0.00	41	4.15	1.30
11	0.50	0.00	42	5.65	1.50
12	0.00	0.00	43	5.15	1.50
13	4.50	0.50	44	4.65	1.50
14	4.25	0.50	45	4.15	1.50
15	4.00	0.50	46	3.65	1.50
16	3.75	0.50	47	3.00	1.50
17	3.50	0.50	48	4.65	2.00
18	3.00	0.50	49	4.15	2.00
19	4.50	0.70	50	3.65	2.00
20	4.15	0.70	51	2.50	2.00
21	3.65	0.70	52	1.50	2.00
22	4.50	0.90	53	5.65	3.00
23	4.25	0.90	54	4.65	3.00
24	4.00	0.90	55	3.65	3.00
25	3.75	0.90	56	2.50	3.00
26	3.50	0.90	57	1.50	3.00
27	3.00	0.90	58	4.65	4.00
28	2.50	0.90	59	3.65	4.00
29	2.00	0.90	60	2.50	4.00
30	1.50	0.90	61	4.65	4.90
31	0.50	0.90			

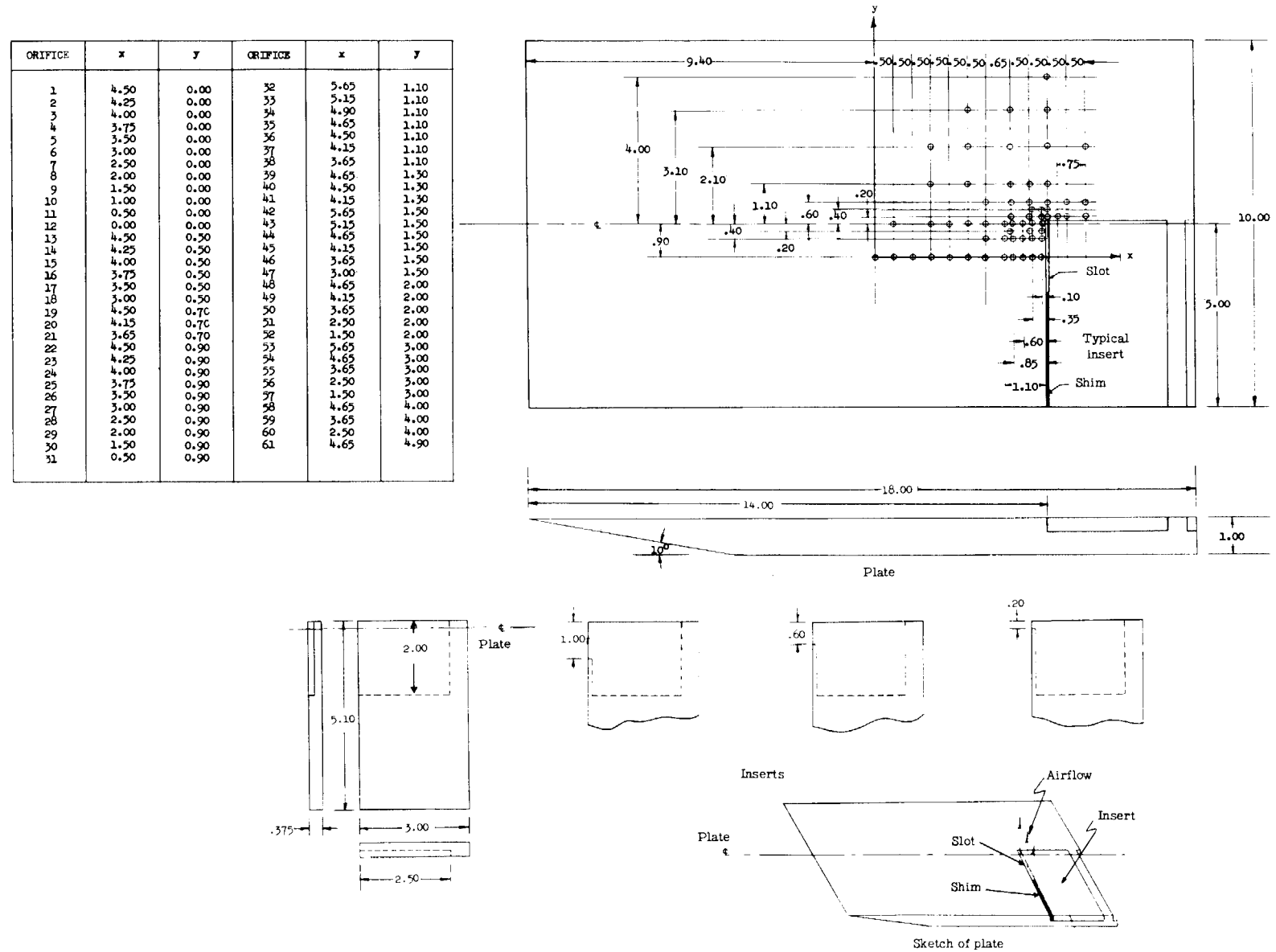

Figure 1.- Model, inserts, and orifice coordinates.

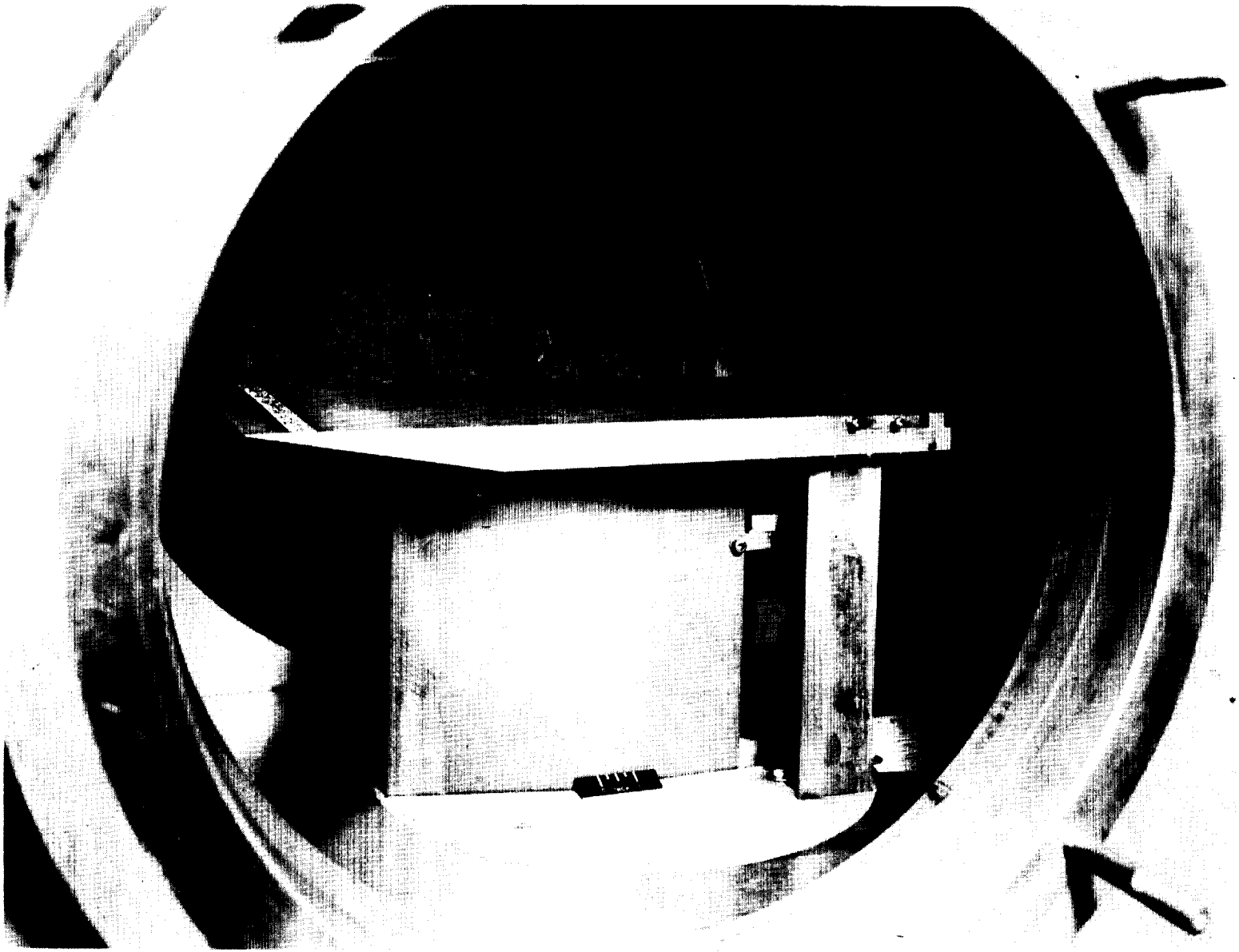

Figure 2.- Model mounted in tunnel. L-61-272

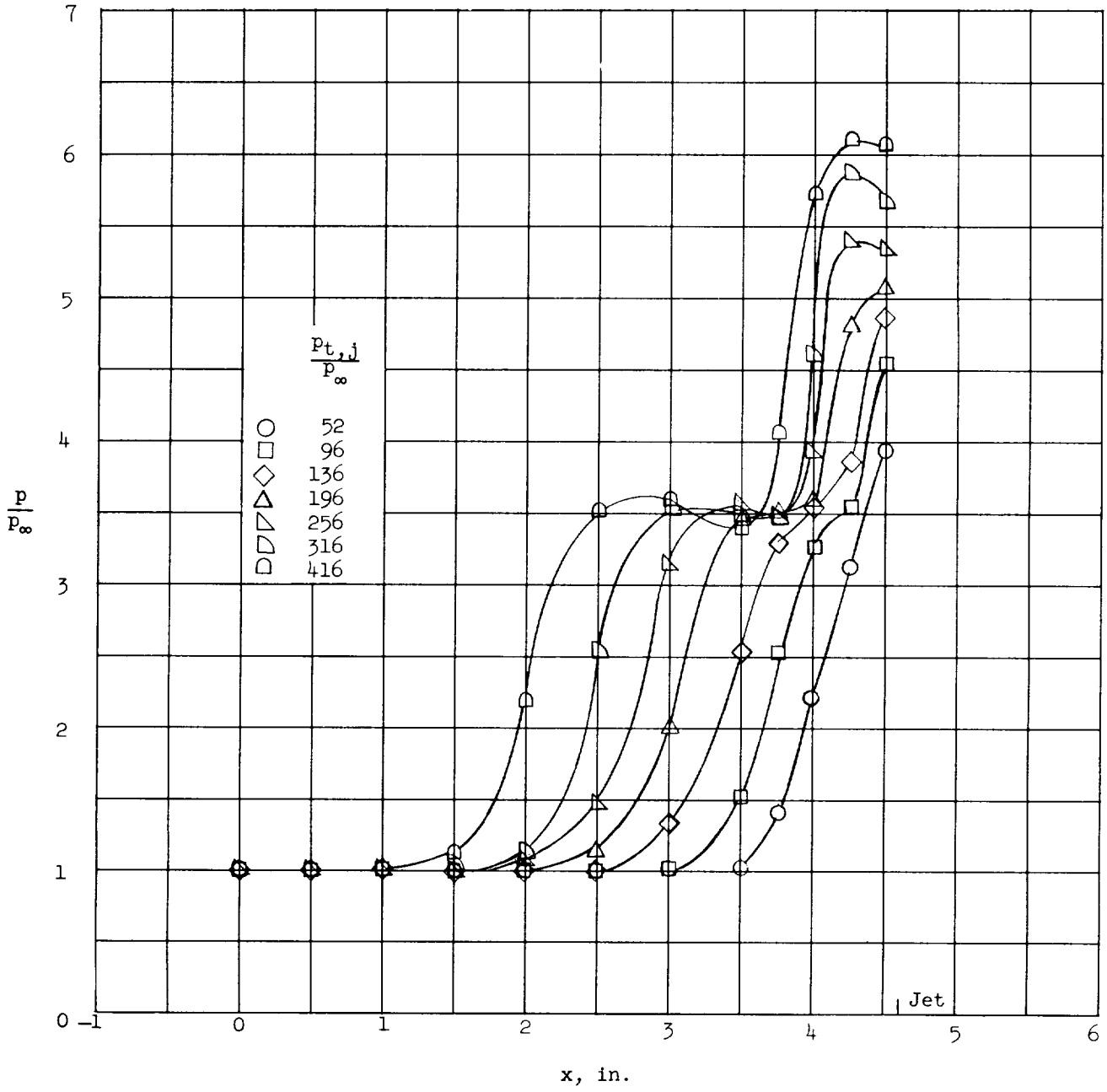

Figure 3.- Typical center-line pressure distribution ahead of rectangular sonic jet for various jet pressure ratios. d = 0.02 inch; s = 2.00 inch.

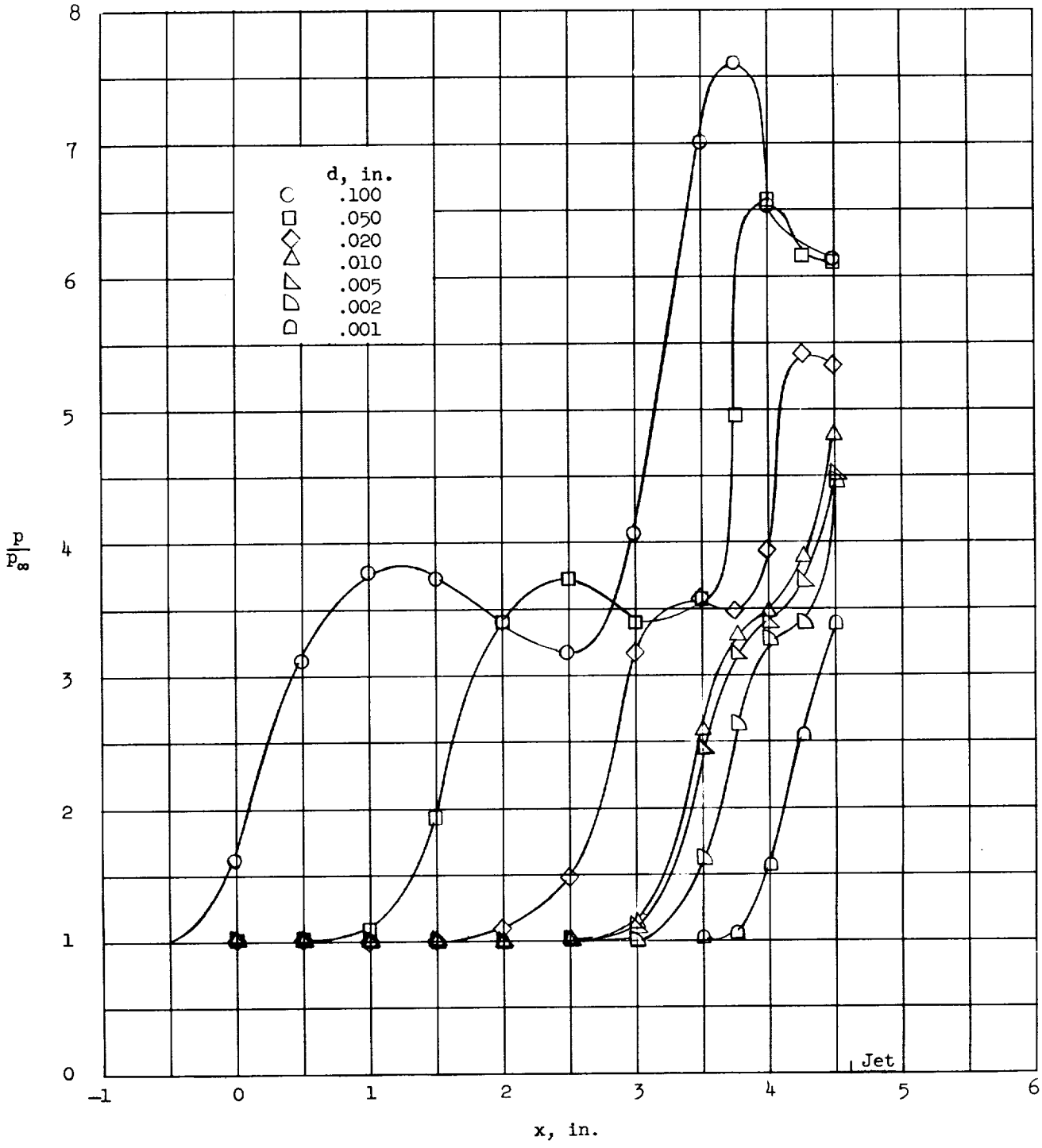

Figure 4.- Typical center-line pressure distribution ahead of a rectangular sonic jet for various jet slot widths. $p_{t,j}/p_\infty = 260$; s = 2.00 inch.

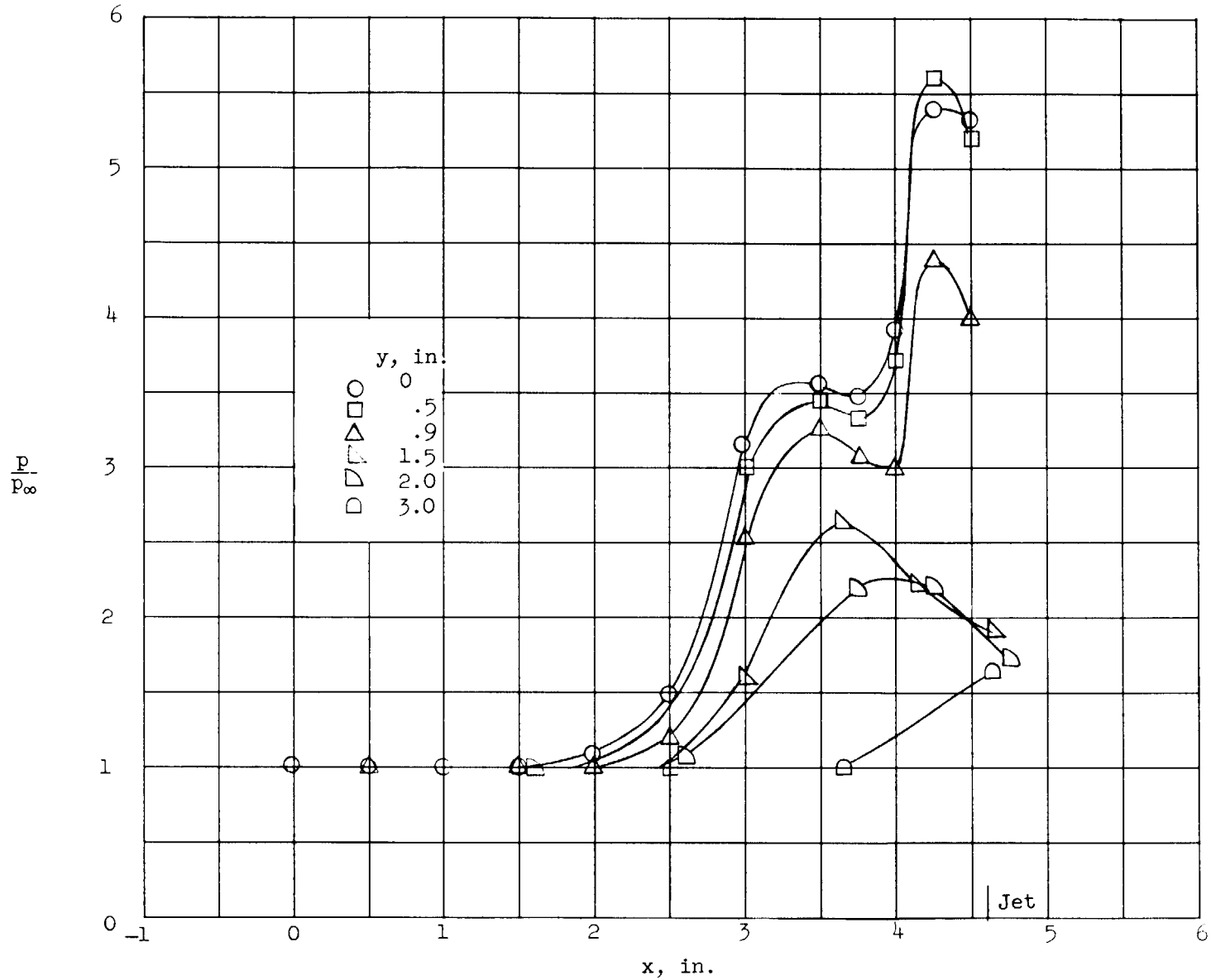

Figure 5.- Typical pressure distribution ahead of a rectangular sonic jet for different spanwise orifice locations. $p_{t,j}/p_\infty$ = 260; d = 0.02 inch; s = 2.00 inch.

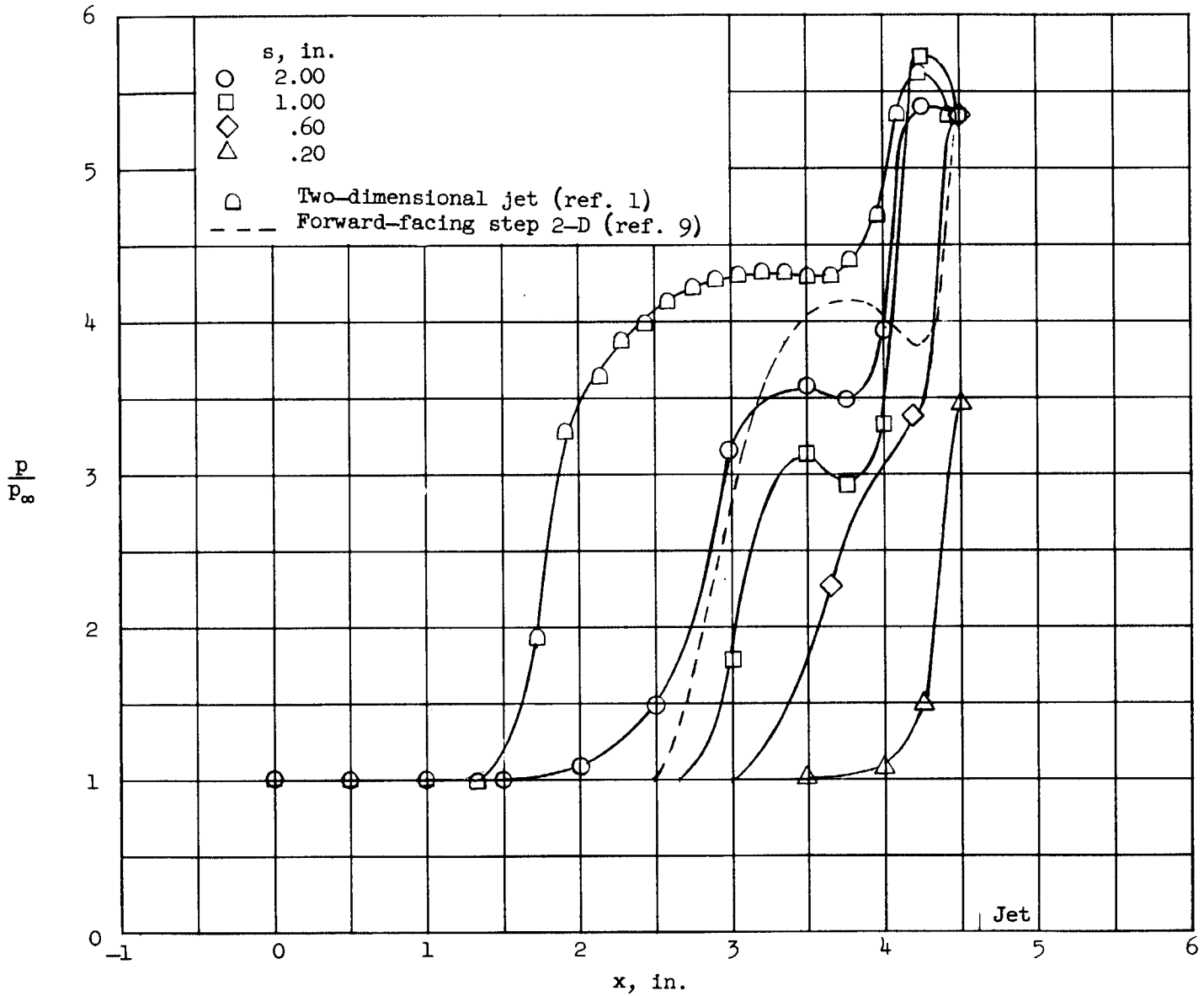

Figure 6.- Typical center-line pressure distribution ahead of a rectangular sonic jet for various jet slot spans. $p_{t,j}/p_\infty = 260$; d = 0.02 inch.

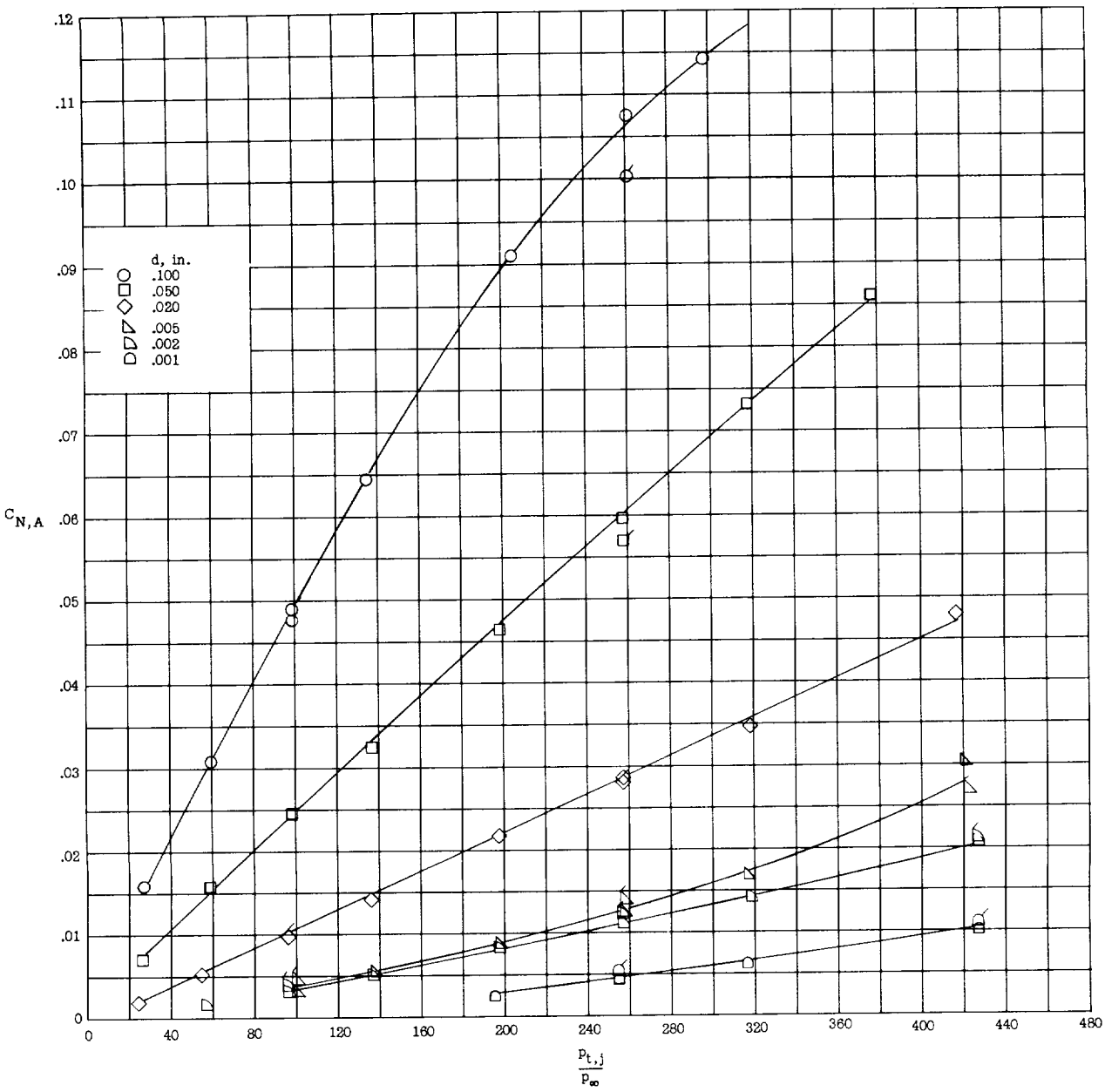

(a) s = 2.00 inches.

Figure 7.- Effect of jet pressure ratio on aerodynamic normal-force coefficient over a range of jet slot widths. Flagged symbols are for values obtained by mechanical integration.

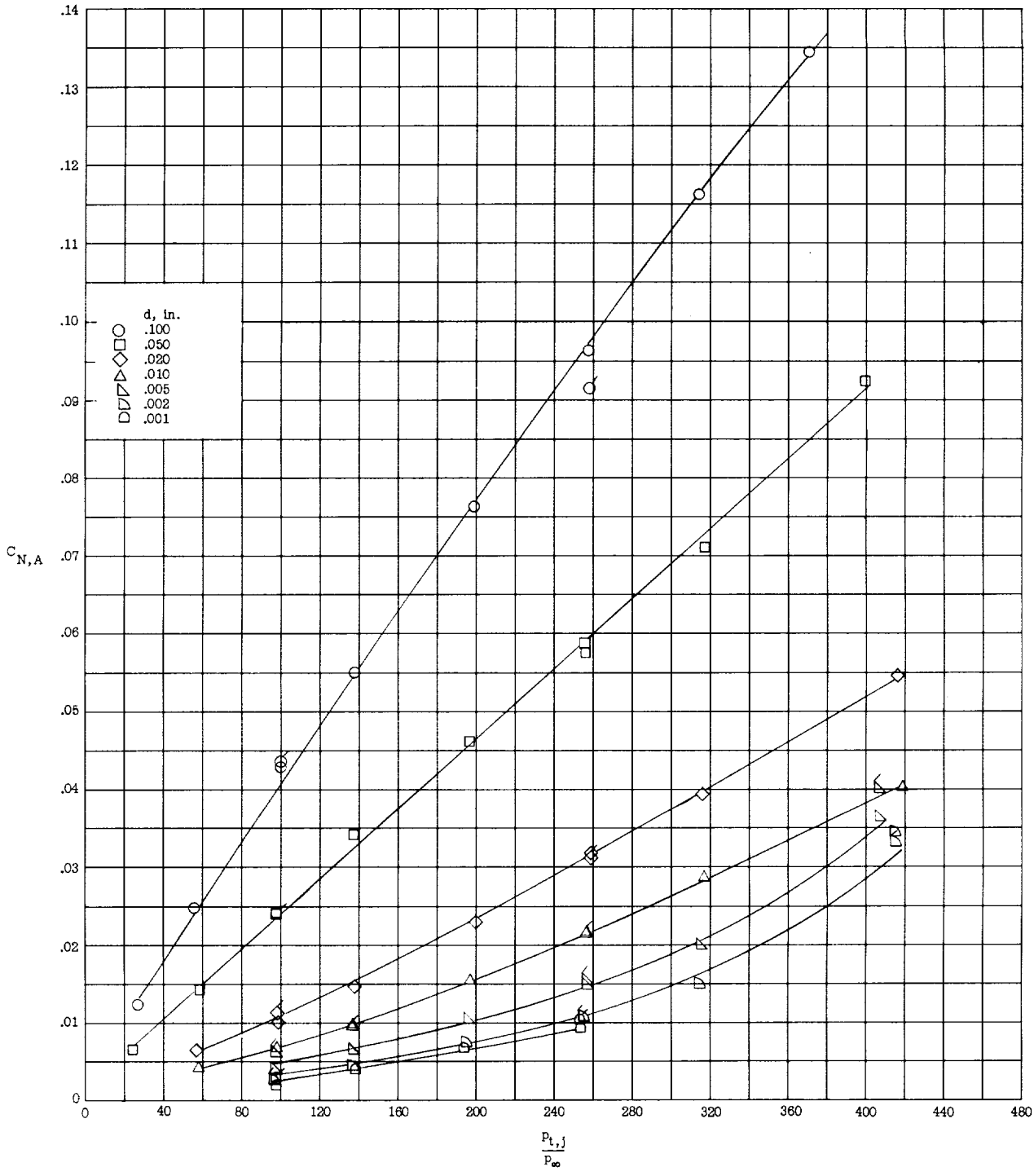

(b) s = 1.00 inches.

Figure 7.- Continued.

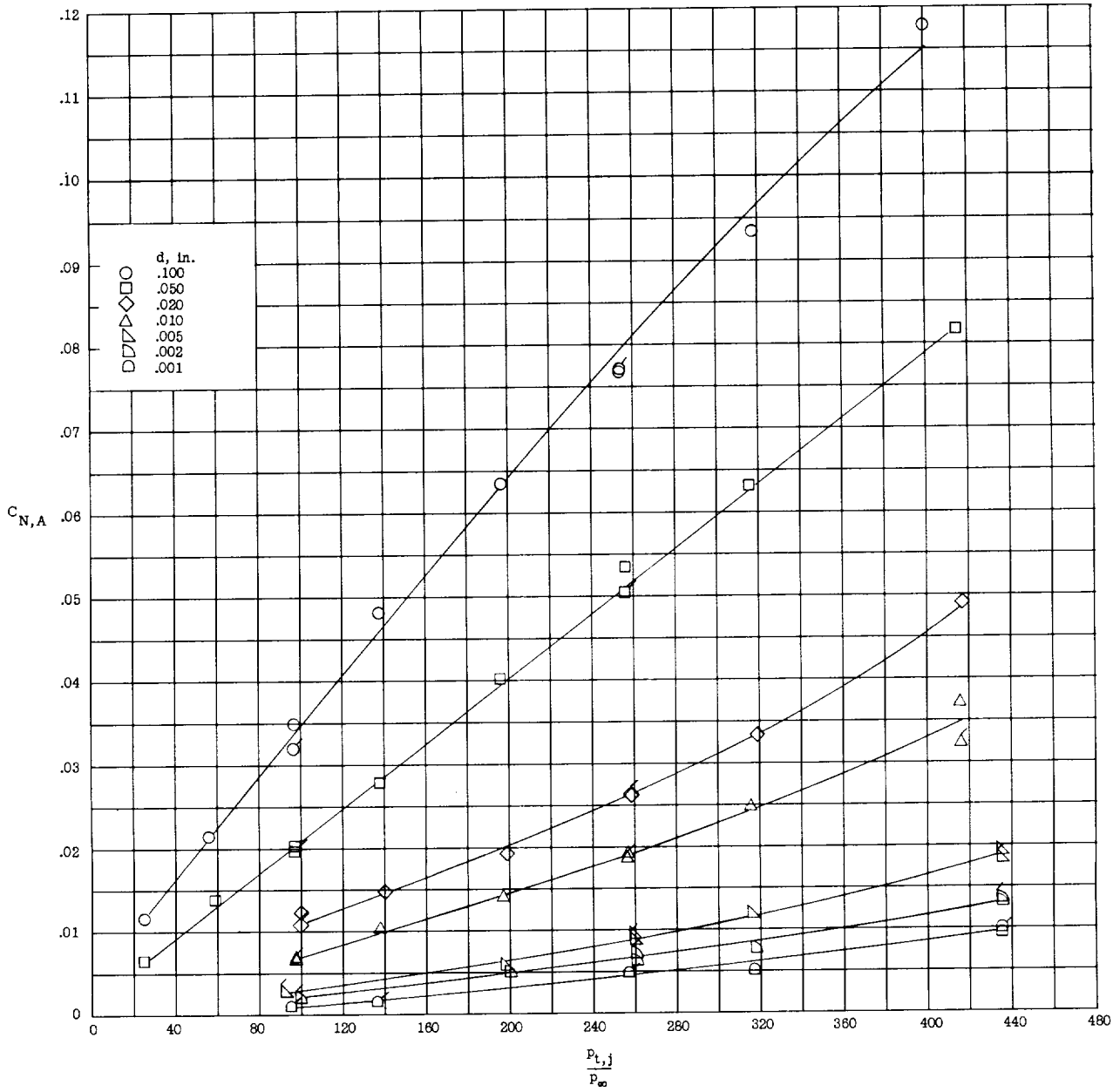

(c) s = 0.60 inch.

Figure 7.- Continued.

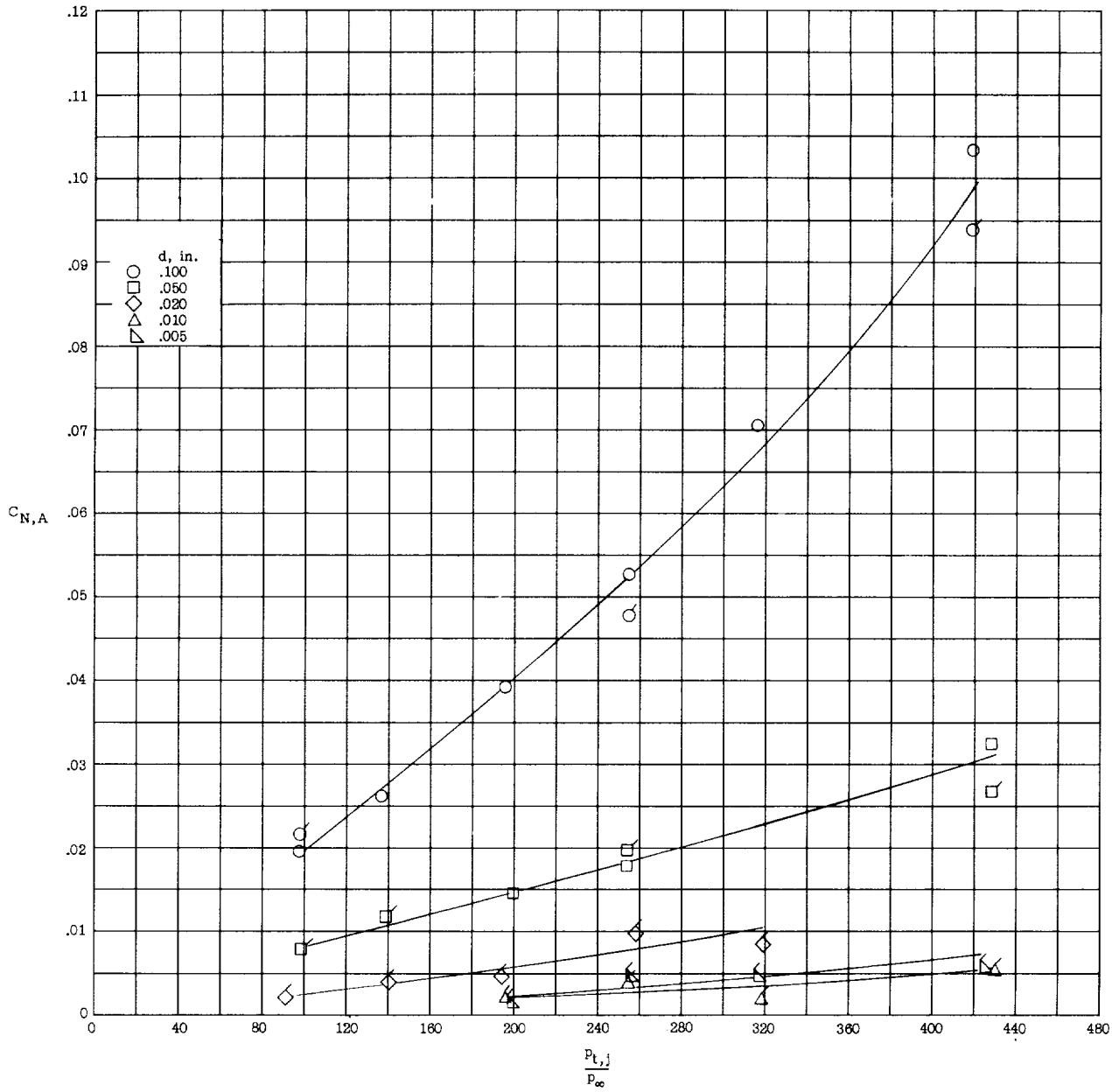

(d) s = 0.20 inch.

Figure 7.- Concluded.

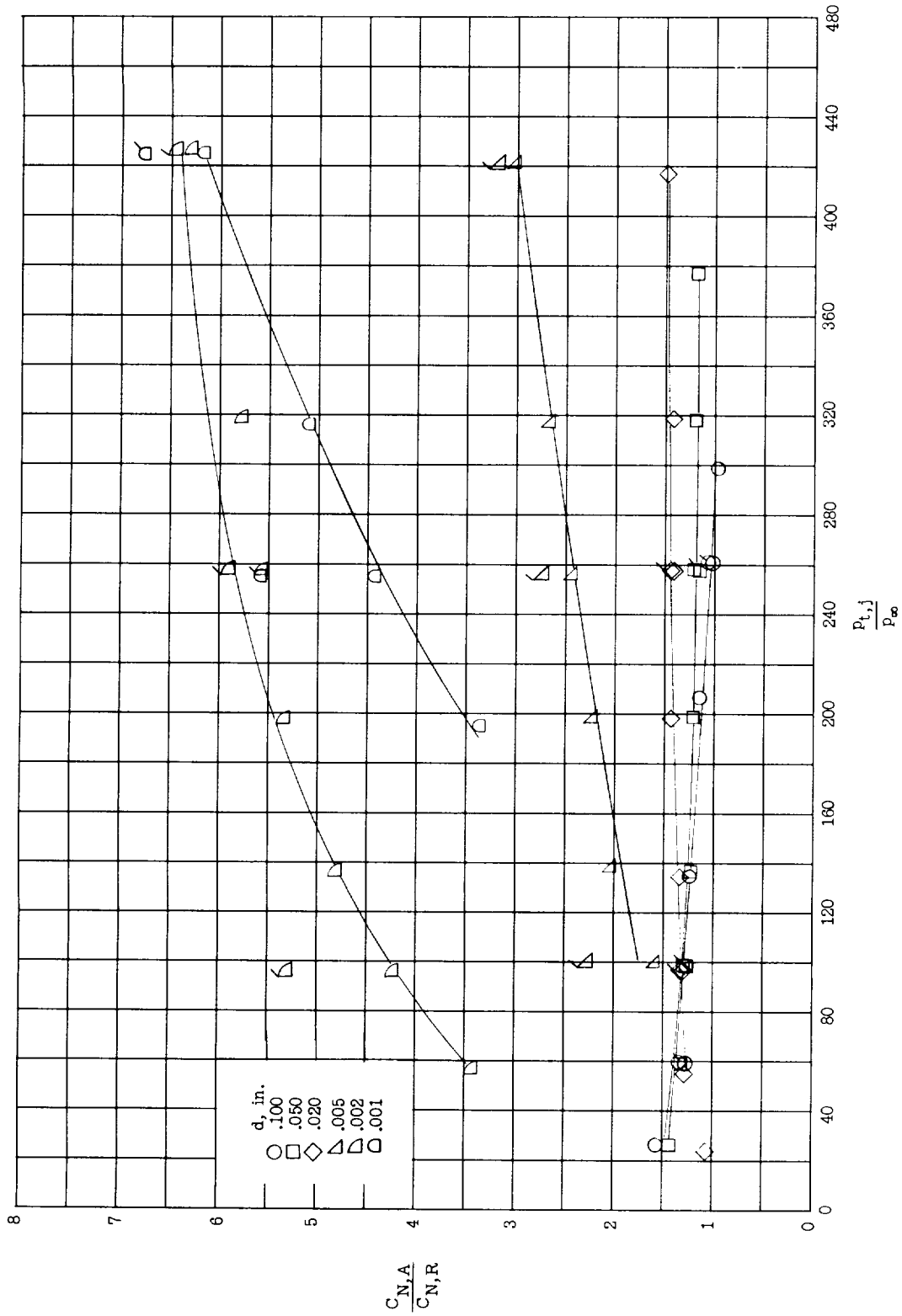

(a) s = 2.00 inches.

Figure 8.- Effect of jet pressure ratio on ratio of aerodynamic to reaction normal-force coefficients over a range of jet slot widths. Flagged symbols are for values obtained by mechanical integration.

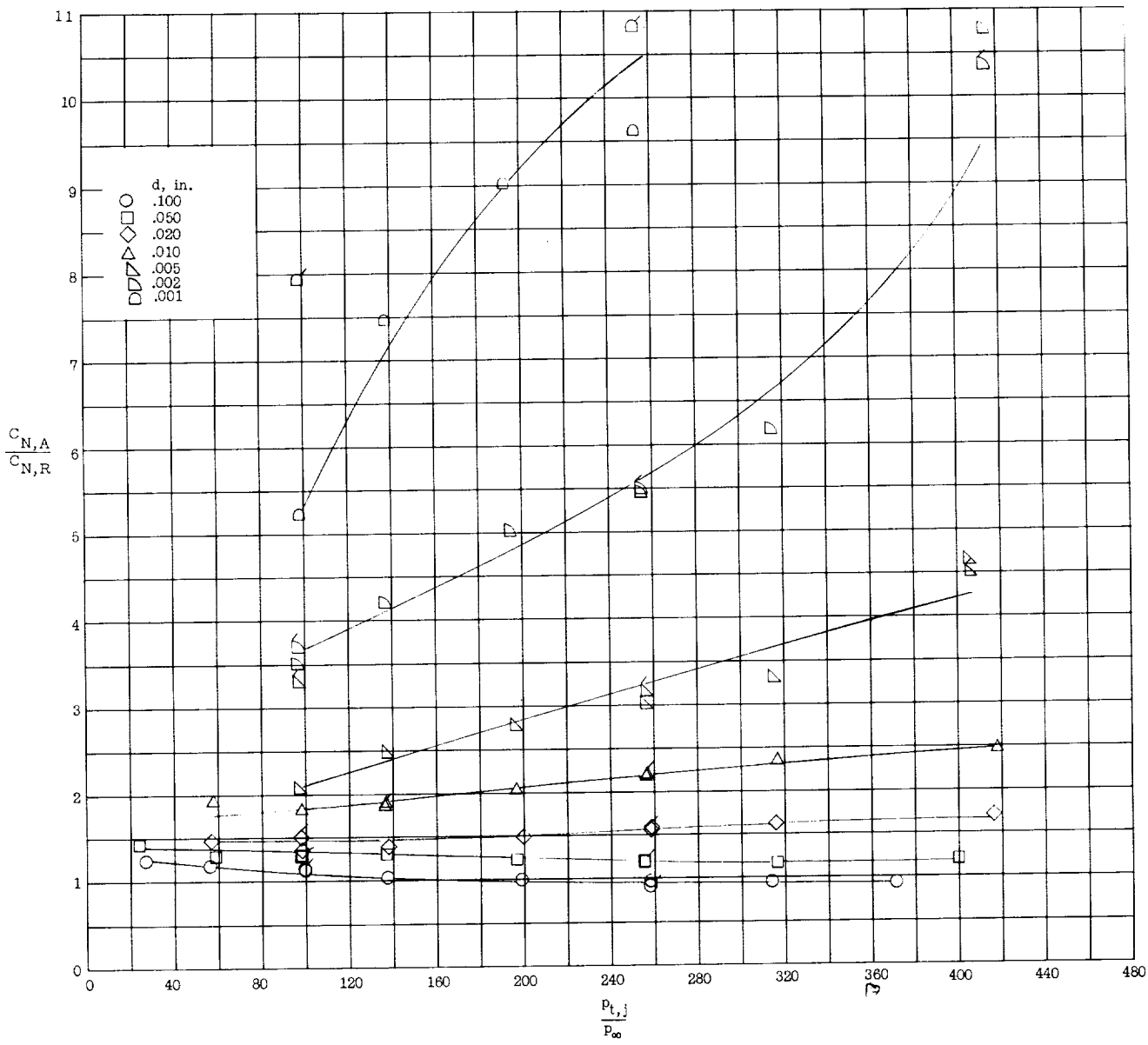

(b) s = 1.00 inch.

Figure 8.- Continued

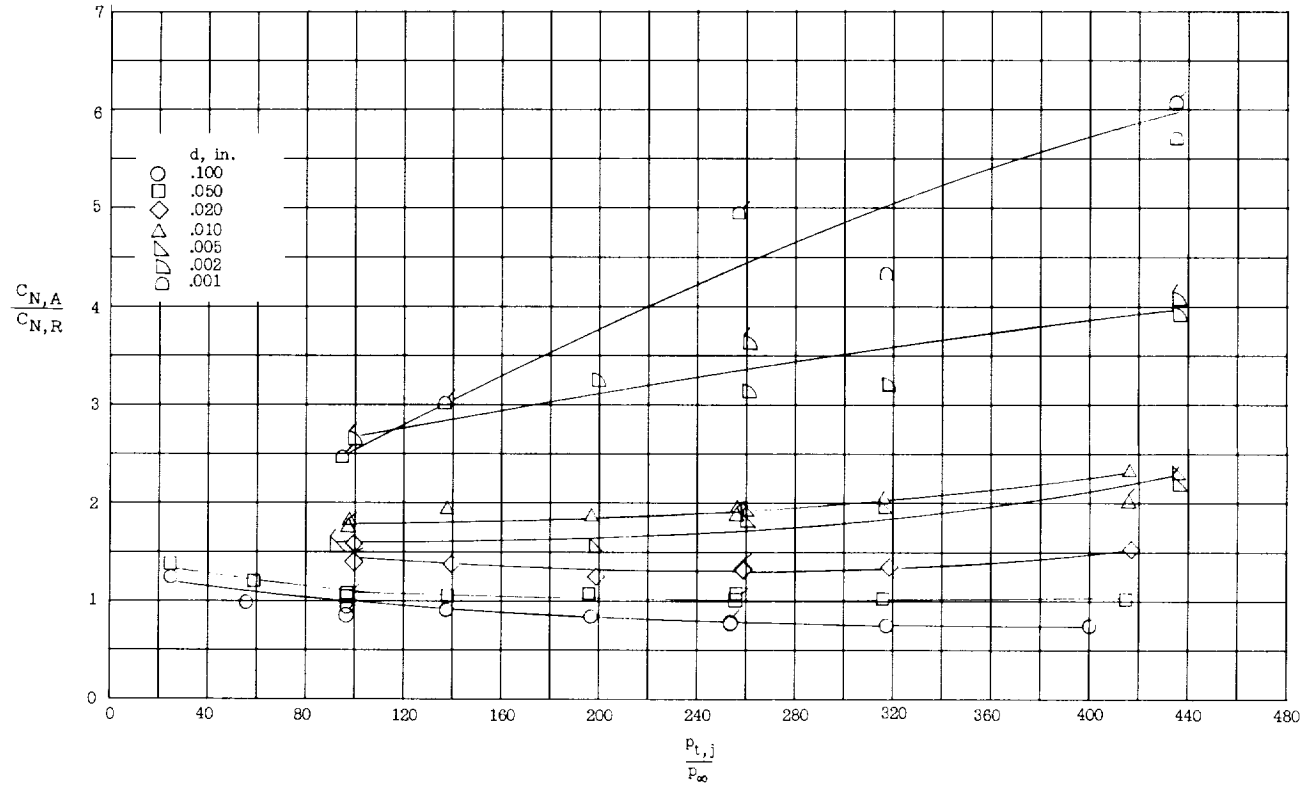

(c) s = 0.60 inch.

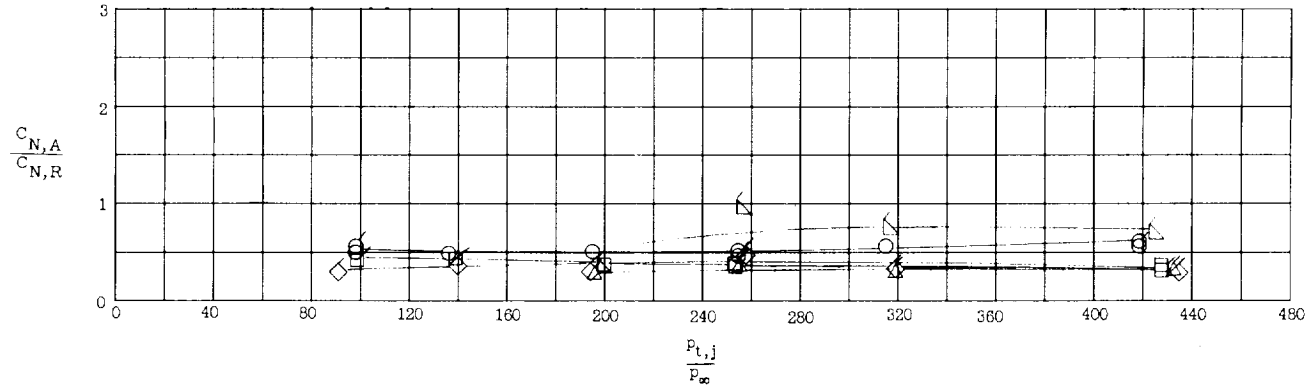

(d) s = 0.20 inch.

Figure 8.- Concluded.

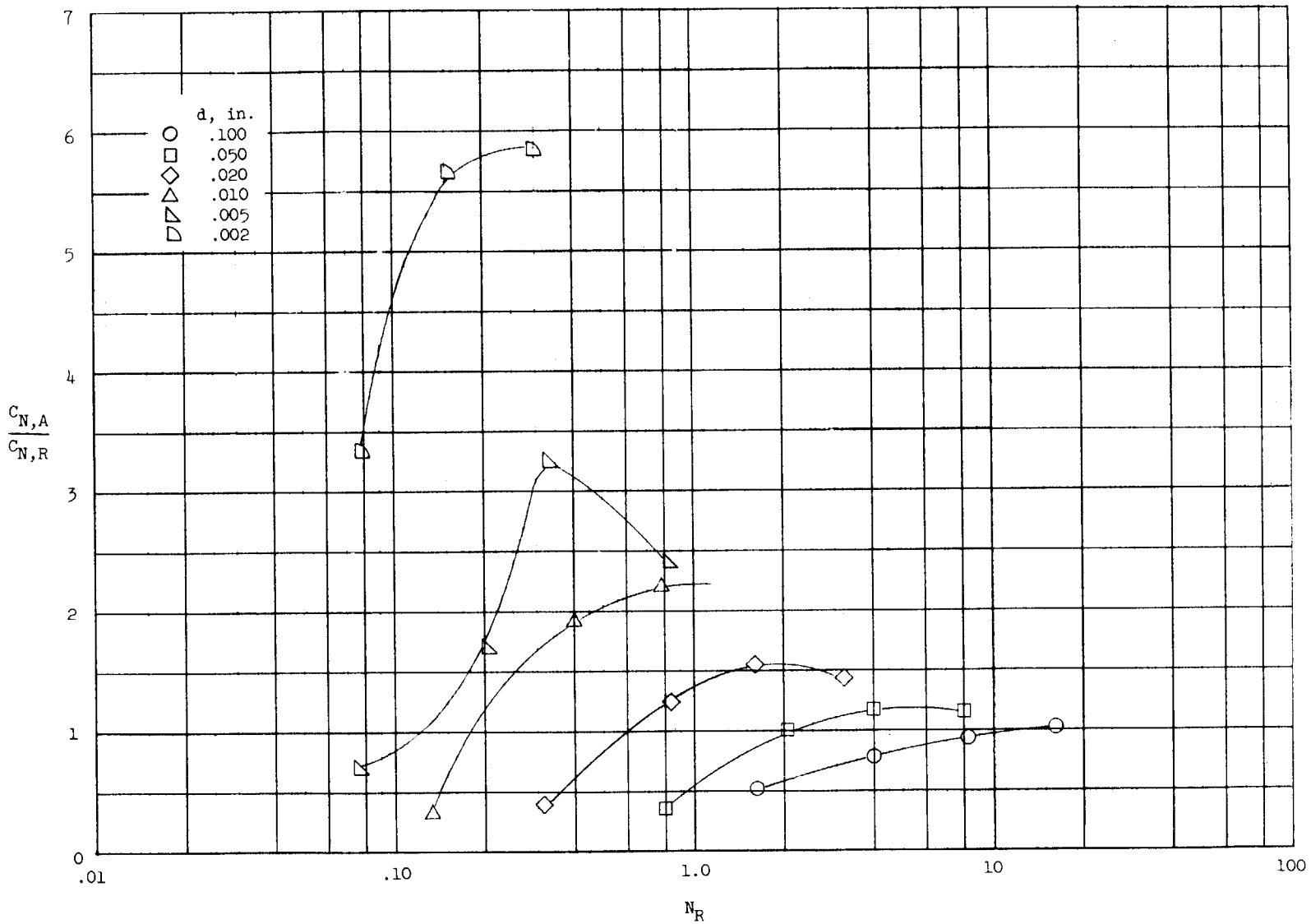

Figure 9.- Variation of ratio of aerodynamic normal-force coefficient to pure reaction normal-force coefficient as a function of pure jet reaction normal force for various jet slot widths. $p_{t,j}/p_\infty = 260$.

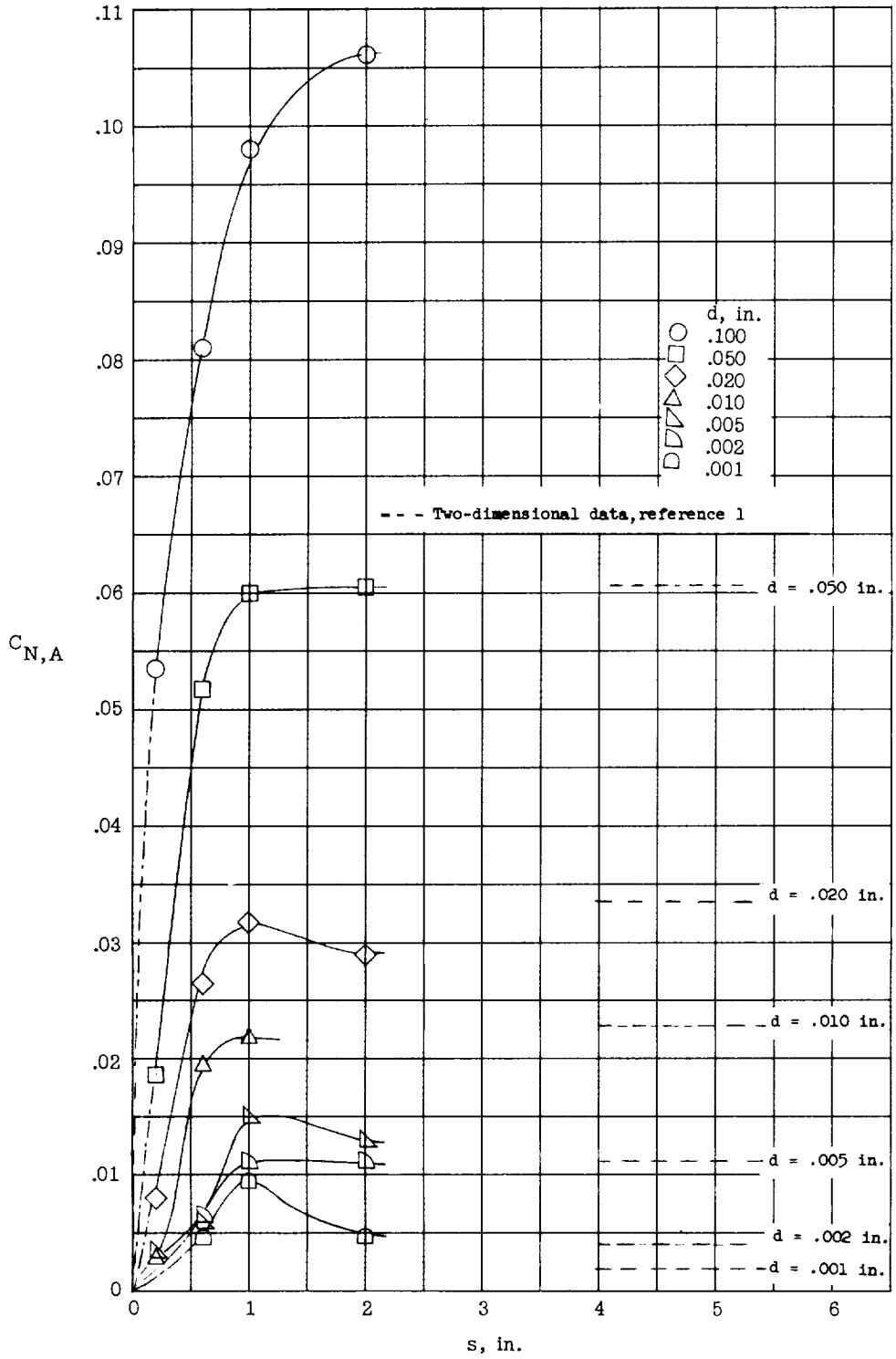

Figure 10.- Effect of jet slot span on aerodynamic normal-force coefficient for the range of slot widths. $p_{t,j}/p_{\infty} = 260$.

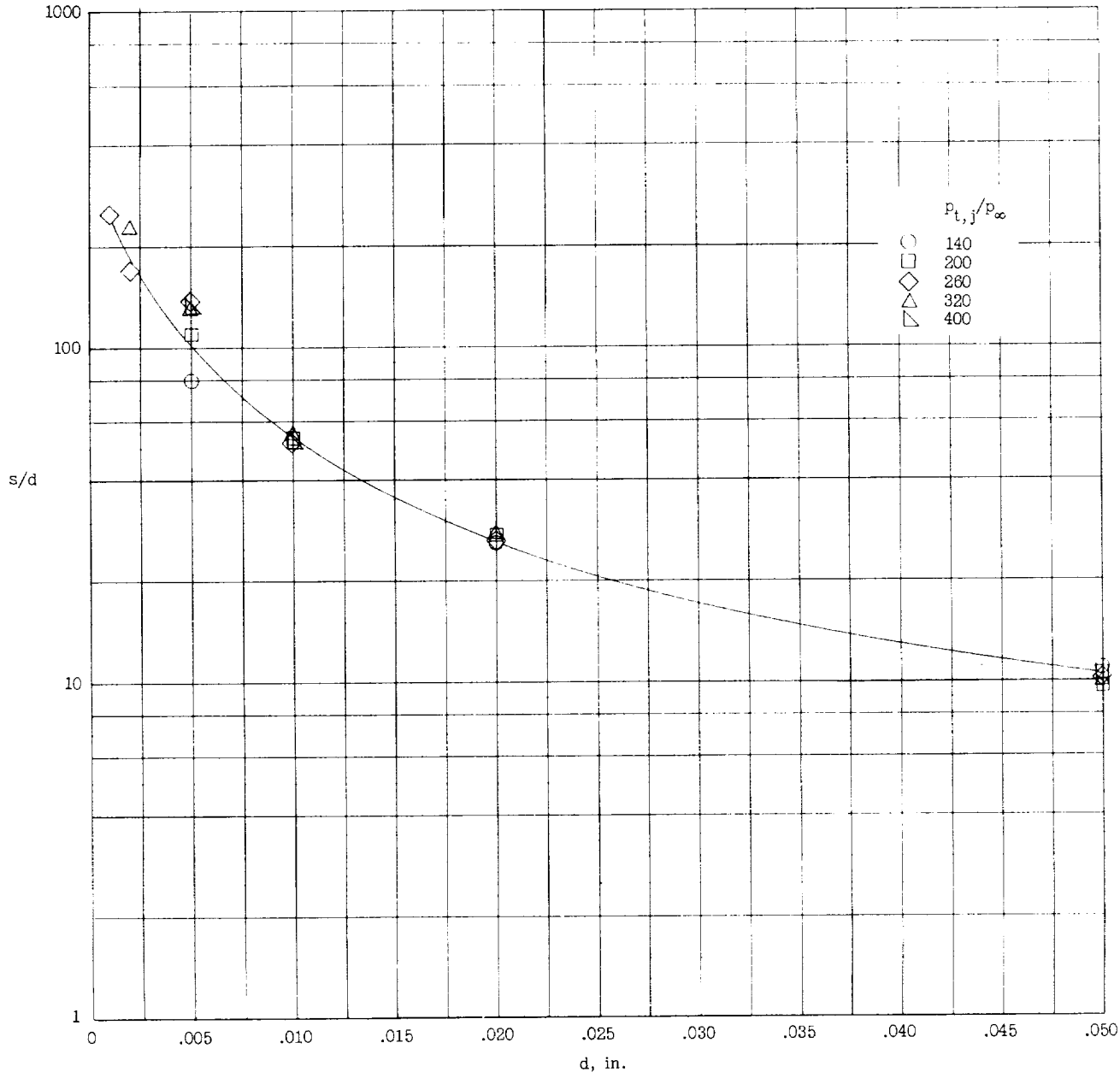

Figure 11.- Effect of jet slot width on aspect ratio where s/d is value at which $C_{N,A}$ is 75 percent of $C_{N,A}$ for a two-dimensional slot for various jet pressure ratios.

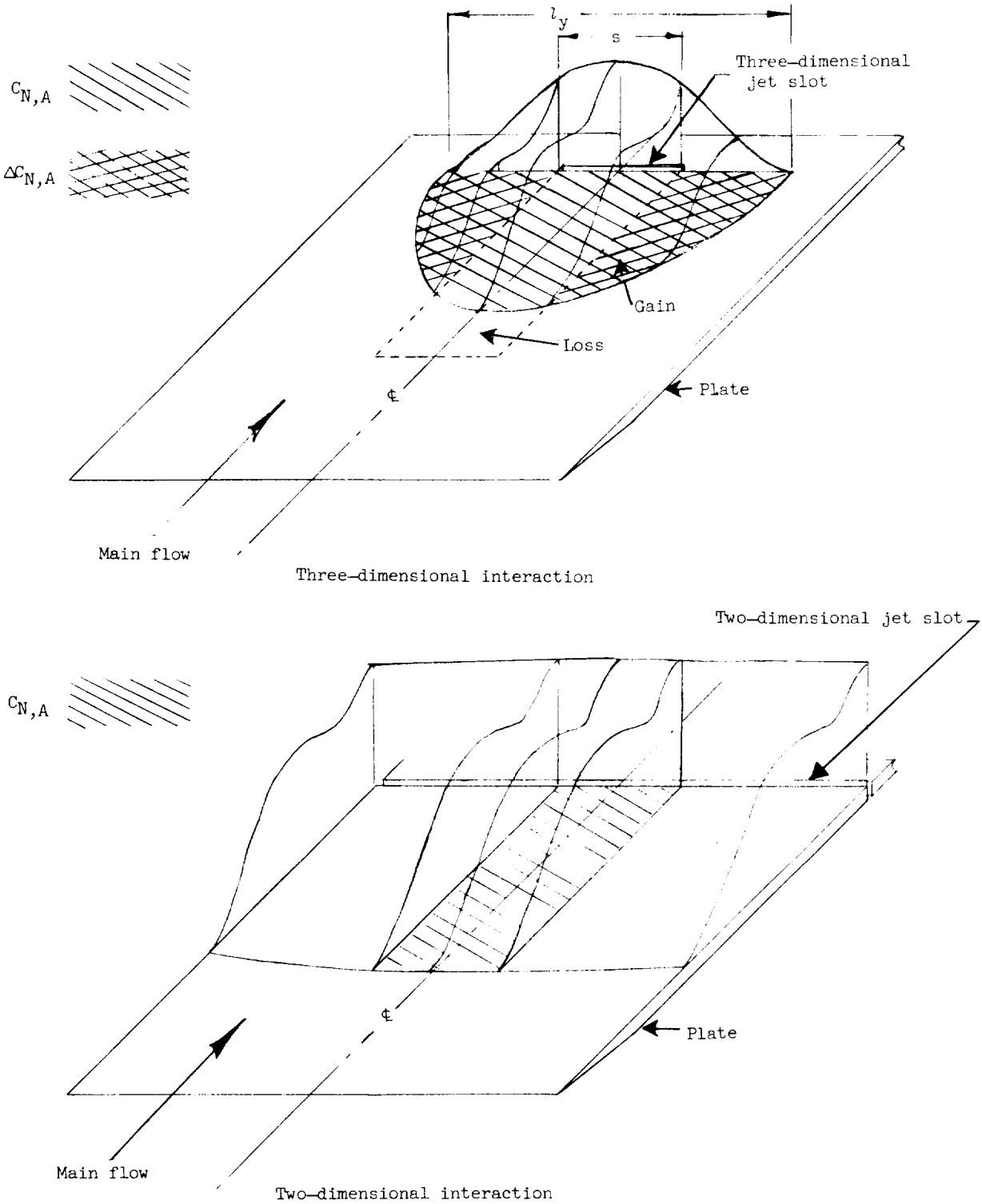

Figure 12.- Sketch of aerodynamic interaction regions for two- and three-dimensional jet slots.

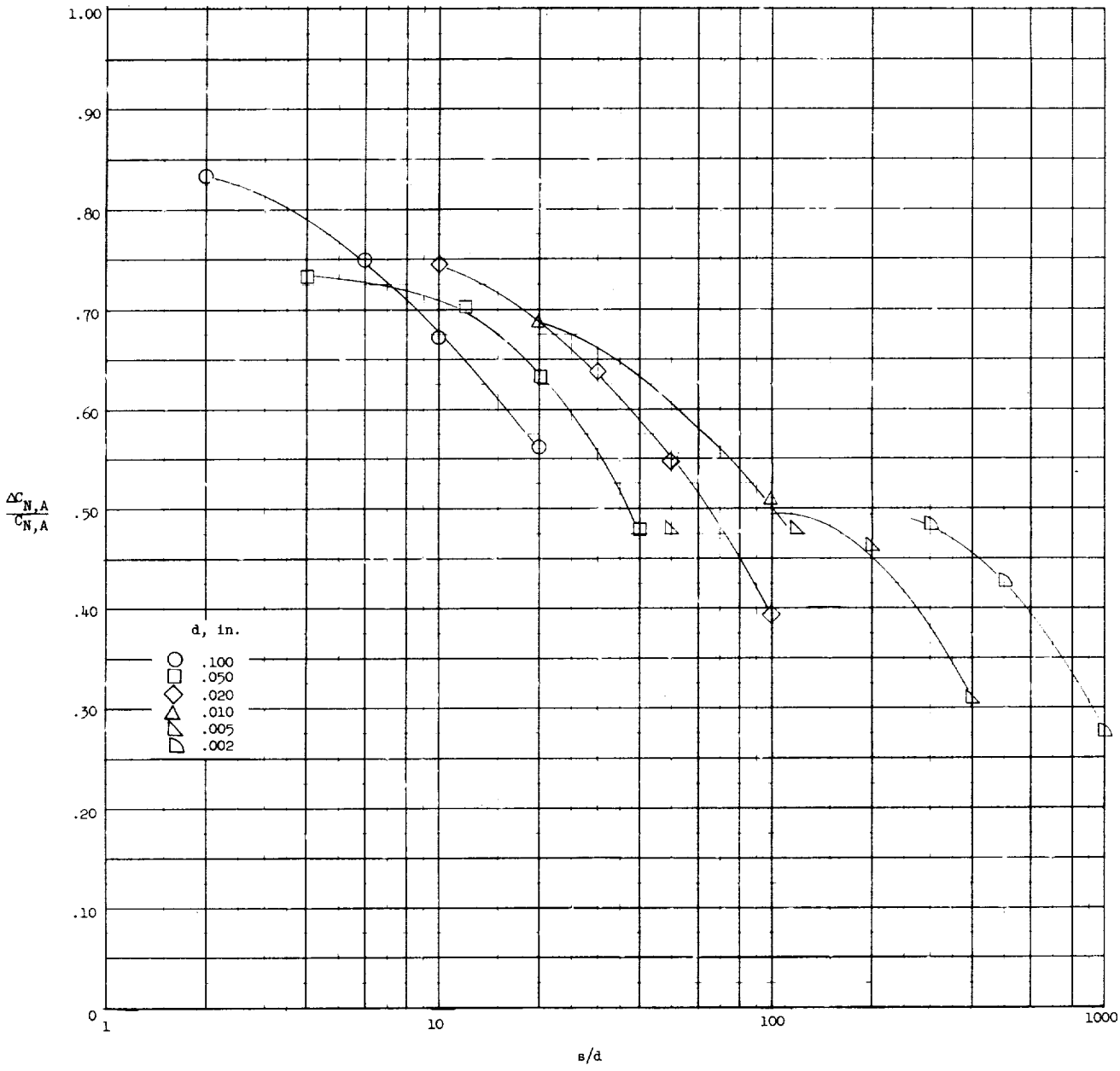

Figure 13.- Effect of aspect ratio on percentage of aerodynamic normal-force coefficient outboard of slot span for various jet slot widths. $p_{t,j}/p_\infty = 260$.

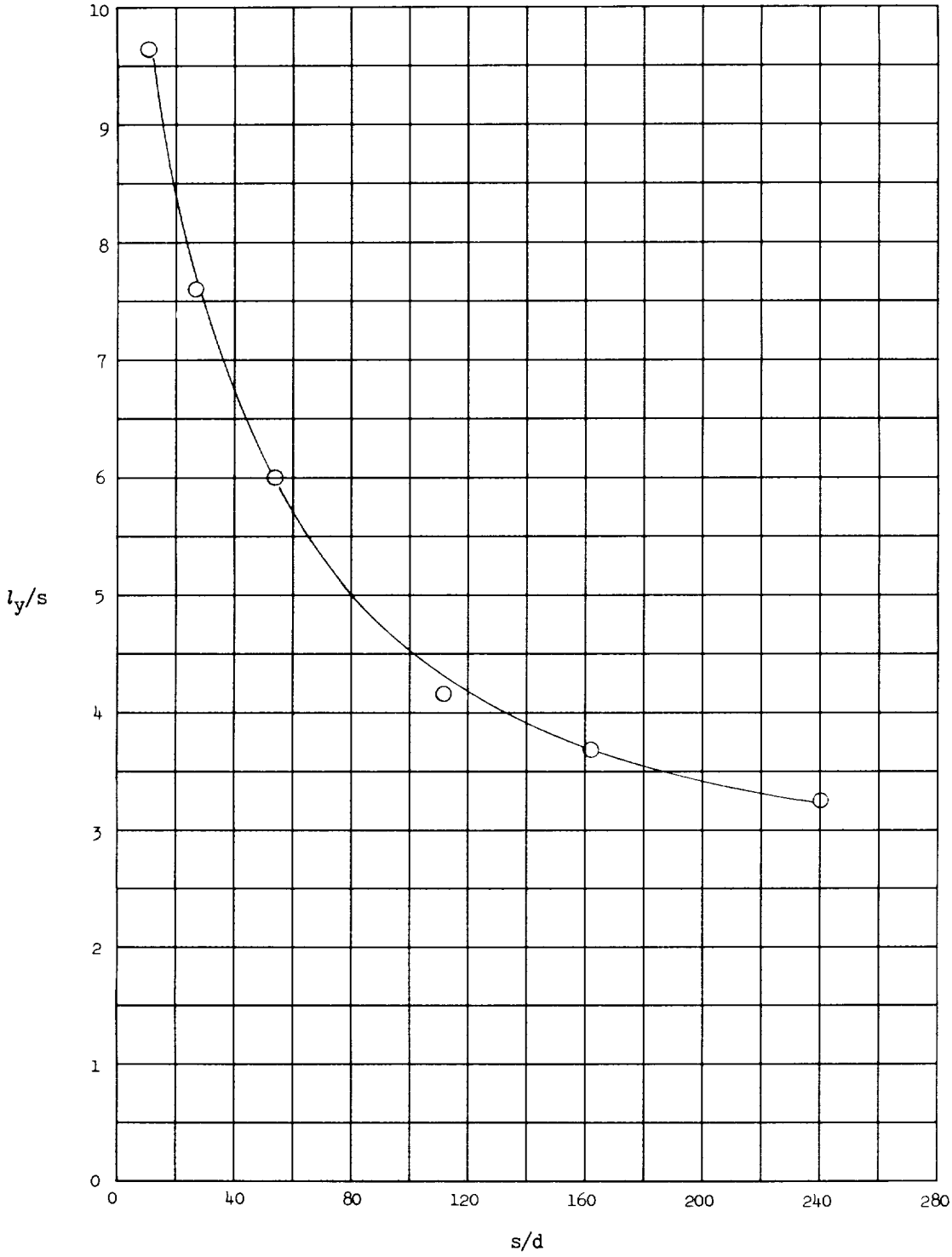

Figure 14.- Effect of jet slot aspect ratio on the amount of minimum surface span needed to obtain full effect of three-dimensional slot.